Preprints of the 19th World Congress
The International Federation of Automatic Control
Cape Town, South Africa. August 24-29, 2014

Automatic controller tuning for soft sensor based flow rate control

S. Leonow * **M. Mönnigmann** *

* *Automatic Control and Systems Theory, Ruhr-Universität Bochum, 44801 Bochum, Germany (e-mail: sebastian.leonow@rub.de, martin.moennigmann@rub.de).*

Abstract: Pumps are often operated poorly controlled and manually throttled, which results in a significantly reduced energy efficiency. We propose an automatic PID controller tuning approach in combination with a dynamic flow rate estimation algorithm for low speed radial pumps to replace expensive flow rate measuring equipment. Since our approach is fully automated, there is minimal additional effort for the customer to implement an automatic flow rate control.

Keywords: soft sensing, radial pump, robust PID, time-delay

1. INTRODUCTION

Pumps contribute significantly to the world wide energy consumption. In the European Union, for example, pumps are responsible for about 16% of the electromotoric power consumption in the service sector (Almeida et al. (2003)). Despite the significant increase in energy efficiency that can be obtained with automatic control (Ferreira et al. (2003)), many pumps are poorly controlled.

Automatic control of pumps is unpopular among practitioners, since it requires sensors, which result in unacceptable additional costs. We have recently reviewed existing flow rate estimation methods and presented a dynamic flow rate estimation method that uses soft sensors in Leonow and Mönnigmann (2013). The proposed soft sensors can easily be integrated into the pumping unit and a flow rate sensor is therefore obsolete.

A second reason for the lack of popularity of automatic control solutions in practice is the need for controller tuning. Even in those cases that do not require any sophisticated method, practitioners often attempt to avoid the controller tuning step and opt for a simple solution such as overdesigning and manual throttling. Among the variety of PID tuning rules, the Ziegler-Nichols and the Chien-Hrones-Reswick empirical rules seem to be most widely known. Recent analytical tuning approaches handle deadtime explicitly in first (Cvejn (2011)) or second order plus deadtime systems (Wang et al. (1999)). A comprehensive approach by Hohenbichler (2009) calculates the stabilizing PID parameter region for arbitrary systems with deadtime, though without regarding closed loop control quality. We present an automatic PID tuning method that is based on the root locus plot and handles deadtime explicitly for strictly delayed processes of arbitrary degree. We apply the tuning approach in combination with the flow rate estimation algorithm presented in Leonow and Mönnigmann (2013) and show that the tuning method can be automated and therefore used by practitioners with little or no background on controller tuning. Despite its simplicity of use, the proposed method guarantees a prespecified closed loop behavior for delayed systems of arbitrary degree, also those with dominant deadtime.

We briefly summarize flow rate estimation in section 2.1. Section 3 describes the automatic process identification method. In section 4 we present the automatic controller synthesis for a class of process models that typically occur in flow rate control. The control performance is evaluated on a real process in section 5, followed by a short conclusion.

2. FLOW RATE ESTIMATION

Numerous flow rate estimation methods have been developed. Recent contributions to this topic were made e.g. by Ahonen et al. (2012). We reviewed this and other methods in Leonow and Mönnigmann (2013) and proposed the *boundary curve method* as a new flow rate estimation algorithm with improved steady state and transient performance. We briefly summarize this method, since it provides the motor current sensor model (1) required by the process identification in section 3.

2.1 Boundary curve method

The boundary curve method is a dynamic flow rate estimation method that is based on the effective value of the stator current $i_{\mathrm{meas}}(t)$, a measurement which is typically provided by the frequency converter. Essentially, two limiting cases of the pumping system are analyzed: The lower limit is defined by the pump operating against a closed discharge valve, which leads to zero flow rate $q = 0$ and a low stator current $i_{\mathrm{meas}}(t)$. The upper limit is defined by the maximum flow rate $q = q_{\max}$ that can be achieved without cavitation and leads to a high stator current. Both limiting cases are captured by *boundary curves*, which are used to estimate steady state parameters. The boundary curves can be determined automatically by a series of

⋆ This research was funded by the Deutsche Bundesstiftung Umwelt DBU.

measurements carried out by the pump itself (Leonow and Mönnigmann, 2013). In addition to measuring and estimating steady state parameters, step responses are used to determine a dynamic model of the motor current sensor, i.e., the relation between the rotational speed $n(t)$ and the measured motor current $i_{\text{meas}}(t)$. The effect of fluid inertia is canceled by setting $q = 0$. A first order plus deadtime model

$$T_L \frac{d\, i_{\text{meas}}(t)}{dt} + i_{\text{meas}}(t) = K\,(n, q) \cdot n(t - T_D) \qquad (1)$$

is sufficient in our case to model the sensor dynamics. $K\,(n, q)$ is a nonlinear function that is estimated from steady state data. The constant parameters T_L and T_D can be identified from step responses (see Leonow and Mönnigmann (2013) for details).

3. PROCESS MODEL FOR CONTROLLER SYNTHESIS

Section 3.1 describes the type of hydraulic process treated here. All requirements stated in section 3.1 apply throughout the paper.

3.1 Process layout and definitions

Consider the layout shown in Fig. 1. The low speed radial pump is operated with rotational speed n and delivers a discharge pressure $p_D = p_1$ to the downstream process. The pump inlet pressure is denoted p_0. The process is modeled as circular pipe with average radius R, length L, inner surface roughness k_S and geodetic heights z_1, z_2 at its inlet and outlet, respectively. The fluid is assumed to be incompressible with constant density ρ and constant kinematic viscosity ν. These assumptions are appropriate, for example, for low speed radial pumps and aqueous media. Note that the assumptions imply that the fluid velocity c is independent of x.

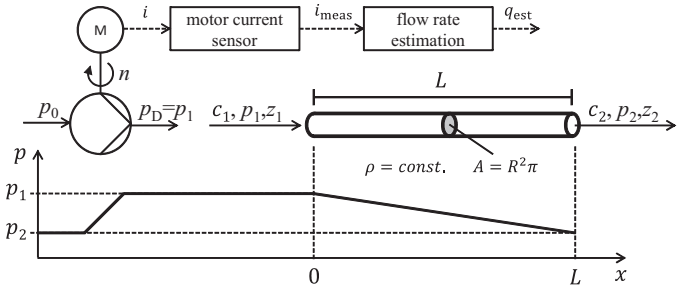

Fig. 1. Process layout.

The process is assumed to be strictly delayed (compare Fig. 2). Consequently, the plant transfer function $G_P(s)$ (12) does not have any zeroes and only negative real poles. The mechanical rotational inertia of the pump is neglected. Its effect is implicitly contained in the parameters T_L and T_D in (1).

3.2 Process modeling

Pipe system: We apply the Bernoulli equation for incompressible, instationary pipe flow

$$p_1(t) + \frac{\rho \cdot c_1(t)^2}{2} + \rho \cdot g \cdot z_1 = p_2(t) + \frac{\rho \cdot c_2(t)^2}{2} + \ldots$$
$$\ldots \rho \cdot g \cdot z_2 + \Delta p_f + \rho \int_0^L \frac{dc}{dt} dx \qquad (2)$$

(Gulich (2007)) to the process described in section 3.1. Since c is independent of x, $\rho c_1^2/2 = \rho c_2^2/2$ and $\int_0^L \frac{dc}{dt} dx = L\,\frac{dc}{dt}$. Furthermore, we introduce $p_2^* = \rho g(z_2 - z_1) + p_2$. Thus (2) implies

$$\rho L \frac{dc(t)}{dt} = \frac{\rho L}{A} \frac{dq(t)}{dt} = p_1(t) - p_2^*(t) - \Delta p_f. \qquad (3)$$

The friction losses Δp_f depend on the fluid parameters ρ, ν, c and on the process parameters R, L and k_S. We use the description due to Darcy (1854) and Weisbach (1845, pp. 136-143)

$$\Delta p_f = \frac{L \cdot \rho}{4 \cdot R} \cdot \lambda_f \cdot \frac{q^2}{A^2}. \qquad (4)$$

Moody (1944) showed that the friction factor $0 < \lambda_f \ll 1$ is approximately constant over a wide flow rate and parameter range. Combining (3) and (4) yields

$$\frac{dq(t)}{dt} = -\frac{\lambda_f \cdot q(t)^2}{4 \cdot R \cdot A} + \frac{A}{\rho L}\left(p_1(t) - p_2^*(t)\right). \qquad (5)$$

Obviously, (5) has the form of a nonlinear first order system. The gain of this system depends on the pipe and fluid parameters, which are determined from measurements in sections 3.3 and 3.4.

Pumping unit: A low speed centrifugal pump with stable q-p_D-characteristic can be described by

$$p_D(t) = C_2 \cdot q(t)^2 + C_0 \cdot \left(\frac{n(t)}{n_{\text{nom}}}\right)^2 + p_0(t) \qquad (6)$$

where n_{nom} is the nominal rotational speed and $C_0, C_2 \in \mathbb{R}$ depend on the pump parameters (see, e.g., Leonow and Mönnigmann (2013)).

An increase in the flow rate $q(t)$ causes an increase in the measured motor current $i_{\text{meas}}(t)$. The response characteristic depends on the motor current sensor only. The motor current sensor model is obtained by using (1) and substituting $n(t)$ with $q(t)$:

$$T_L \frac{d\, i_{\text{meas}}(t)}{dt} + i_{\text{meas}}(t) = K\,(q)\, q(t - T_D). \qquad (7)$$

The parameters T_L and T_D in (7) are known from (1). We note that $q_{\text{est}}(t)$ responds to changes of $i_{\text{meas}}(t)$ immediately, i.e., without delay and without lag of any order (see Leonow and Mönnigmann (2013)).

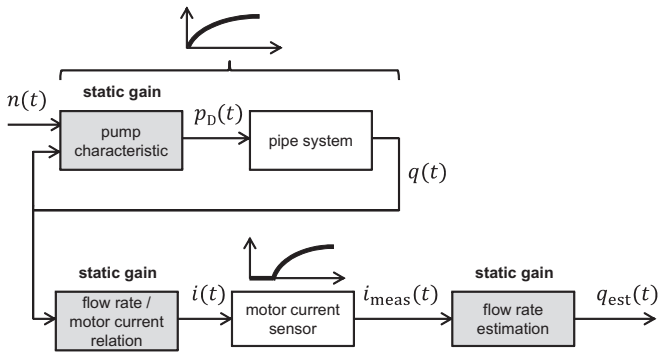

Fig. 2. Process model structure.

Combining (5), (6) and (7) yields the process model sketched in Fig. 2. The response of $q(t)$ to a change in $n(t)$ can be expressed as first order model according to (5) and (6). The response of $q_{\text{est}}(t)$ to a variation in $q(t)$ is expressed by (7) as described above. After linearization the relation between $n(t)$ and $q_{\text{est}}(t)$ is described by an aperiodic second order plus deadtime model (SOPDT).

An aperiodic SOPDT model is uniquely determined by its response to a unit step. The unit step response can conveniently be stated in terms of the physical parameters of the pump and process as follows:

$$\hat{q}(t) = \begin{cases} 0, & t < T_D \\ f_q(K_P, T_D, T_L, T_Q, t), & t \geq T_D \end{cases} \tag{8}$$

with

$$f_q = K_P \left[1 - \frac{1}{T_L - T_Q}\left(T_L e^{-\frac{t-T_D}{T_L}} - T_Q e^{-\frac{t-T_D}{T_Q}}\right)\right], \tag{9}$$

where the deadtime T_D and the pumping unit time constant T_L are known from (1), i.e., the flow rate estimation described in section 2.1. Sections 3.3 and 3.4 describe how to identify the process gain K_P and the fluid acceleration time constant T_Q from a step response.

3.3 Identification of K_P

The gain K_P in (9) can be calculated from

$$K_P = \frac{q_{\text{est,end}} - q_{\text{est,start}}}{n_{\text{end}} - n_{\text{start}}} \tag{10}$$

for $q_{\text{est,start}}$, $q_{\text{est,end}}$, n_{start} and n_{end} from a step response. An example for such a step response is shown in Fig. 4. Since the considered process is nonlinear, K_P depends on the operating point. In order to ensure closed loop stability, the calculation of K_P has to be performed for all typical operating points and the highest K_P must be selected for controller synthesis. We analyze the behavior of K_P for the particular laboratory test setup at the beginning of section 5.

3.4 Identification of T_Q

We determine the remaining unknown parameter T_Q in (9) by solving the least-squares problem

$$\min_{T_Q} \sum_{t_i=T_D}^{t_{\text{end}}} \left(q_{\text{est}}(t_i) - \hat{q}\left(t_i, K_P, T_L, T_Q, T_D\right)\right)^2 \tag{11}$$

where T_L, T_D and K_P are fixed and the time series $q(t_i)$ is a measured step response. This problem has a unique minimum, since (9) is strictly decreasing in $T_Q \in \mathbb{R}^+ \neq T_L$. The discontinuity in (9) at $T_Q = T_L$ can be removed in the sense that the limit from below and above are equal (cf. Fig. 4). The process model (8) is finally expressed by the transfer function

$$G_P(s) = \frac{K_P \cdot e^{-T_D s}}{(T_L s + 1)(T_Q s + 1)} \tag{12}$$

with $K_P, T_L, T_Q \in \mathbb{R}^+$ and $T_D \in \mathbb{R}_0^+$.

4. AUTOMATIC CONTROLLER SYNTHESIS FOR FLOW RATE CONTROL

We consider two control objectives that are popular and often used in practice: The *aperiodic limit control* features the fastest possible setpoint tracking without overshoot (cf. section 4.2). The second objective is the ± 45 deg *control* (cf. section 4.3), which results in a reasonable compromise between speed and robustness, since it leads to a damping $d = 0.707$ in closed loop and thus to a low overshoot and reduced rise time.

4.1 Characteristic equation

Consider the open-loop transfer function of a PID controller and plant of arbitrary degree and with deadtime

$$G_o(s) = \frac{K_C K_P}{D(s)} e^{-T_D s}, \tag{13}$$

where we assume that the slowest plant time constants have been compensated with the controller time constants. [1] The denominator $D(s)$ is polynomial of arbitrary degree $z \in \mathbb{N}$. It consists of the plant denominator $D_P(s)$ with coefficients a_k, multiplied by the integral part of the controller:

$$D(s) = T_C s \cdot D_P(s) = T_C s \cdot \sum_{k=0}^{z-1} a_k \cdot s^k, \; a \in \mathbb{R}^+ \tag{14}$$

All poles $s_o \in \mathbb{R}_0^-$ of $G_o(s)$ are located on the negative real axis in accordance with the assumptions stated in section 3.1. The closed-loop characteristic equation reads

$$C(s) = D(s) + K_C \cdot K_P \cdot e^{-T_D \cdot s} \tag{15}$$

with complex $s = s_R + s_I j$, $K_C, K_P \in \mathbb{R}^+$ and $T_D \in \mathbb{R}_0^+$.

We assume the dominant pair of roots of $D(s)$ remains to be the dominant pair of roots of $C(s)$ for all stabilizing K_C. Due to the complex exponential function $e^{-T_D s}$ in (15), $C(s)$ has an infinite number of roots in the complex plane for $T_D > 0$. Arguably, this is the reason why the root locus method is not popular for deadtime systems. While the construction of the whole root locus plot is tedious in this case, we show in sections 4.2 and 4.3 that the calculation of the aperiodic limit and the ± 45 deg criterion is simple.

4.2 Aperiodic limit control

The aperiodic limit is defined by the largest value of K_C for which the dominant pair of roots of $C(s)$ is real. Due to the factored s in (14) there exists a root $s_1 = 0$ for $K_C = 0$. Let s_2 denote the second rightmost root of $C(s)$ for $K_C = 0$. The roots s_1 and s_2 approach each other for increasing values of K_C, collapse, and become a complex conjugate pair. Let the value at which the two roots collapse be denoted s^*. We claim s^* is the maximum of

$$K_C(s_R) = -\frac{D(s_R)}{K_P \cdot e^{-T_D \cdot s_R}} \tag{16}$$

in the interval $[s_1, s_2]$, which can be seen as follows. $K_C(s_R)$ defined in (16) solves (15) under the assumption that the solution is real, i.e., $s = s_R \in \mathbb{R}$. Since the poles s_1 and s_2 become a complex conjugate pair for larger values of K_C, the largest value of $K_C(s_R)$ defined in (16) that can be attained under the assumption $s_R \in \mathbb{R}_0^-$ corresponds to the double real root s^*.

[1] We apply a PI controller to the SOPDT plant (22) in the application in section 5 but state the more general case here.

4.3 Control with ±45 deg root location

The 45 deg case can be described with similar geometric considerations as the aperiodic one. A complex conjugate pair of roots is located on the ±45 deg locus if and only if $-s_R = s_I$ for one of the complex conjugate roots. The root

$$\tilde{s} = -\sigma + \sigma j,\ \sigma \in \mathbb{R}_0^+ \tag{17}$$

satisfies this criterion. Substituting $\tilde{s}$ into (15) yields

$$\begin{aligned} C(\tilde{s}) = \Re(D(\tilde{s})) + K_C \cdot K_P \cdot e^{T_D \cdot \sigma} \cdot \cos(T_D \cdot \sigma) \\ + \left[\Im(D(\tilde{s})) - K_C \cdot K_P \cdot e^{T_D \cdot \sigma} \cdot \sin(T_D \cdot \sigma)\right] j \end{aligned} \tag{18}$$

Solving $C(\tilde{s}) = 0$ is equivalent to solving both $\Re(C(\tilde{s})) = 0$ and $\Im(C(\tilde{s})) = 0$. K_P can be removed from these equations by solving both $\Re(C(\tilde{s})) = 0$ and $\Im(C(\tilde{s})) = 0$ for K_P and setting the resulting expressions equal. After rearranging and dividing by $e^{T_D \cdot \sigma}$ this yields

$$\Re(D(\tilde{s})) \cdot \sin(T_D \cdot \sigma) + \Im(D(\tilde{s})) \cdot \cos(T_D \cdot \sigma) = 0 \tag{19}$$

The solutions of (19) represent all σ such that $\tilde{s}$ defined in (17) satisfies the 45 deg criterion. Since σ is equal to the distance from $\tilde{s}$ to the imaginary axis, we are looking for the smallest $\sigma^* \in \mathbb{R}_0^+$ that solves (19). The corresponding controller gain $K_C(\sigma^*)$ can be calculated by substituting σ^* into either the real or the imaginary part of (18).

Decomposing $D(\tilde{s})$ from (19) into its real and imaginary part yields

$$\begin{aligned} \Re(D(\tilde{s})) = &\sum_{k=1}^{\lfloor z/4 \rfloor} a_{(4k)} (-4)^k \cdot \sigma^{(4k)} \\ &- \sum_{k=1}^{\lceil z/2 \rceil} a_{(2k-1)} (-1)^{\lfloor k/2 \rfloor} \cdot 2^{(k-1)} \cdot \sigma^{(2k-1)} \end{aligned} \tag{20}$$

and

$$\begin{aligned} \Im(D(\tilde{s})) = &\sum_{k=1}^{\lfloor (z+2)/4 \rfloor} a_{(4k-2)} \frac{(-4)^k}{2} \cdot \sigma^{(4k-2)} \\ &+ \sum_{k=1}^{\lceil z/2 \rceil} a_{(2k-1)} (-1)^{\lfloor (k-1)/2 \rfloor} \cdot 2^{(k-1)} \cdot \sigma^{(2k-1)}, \end{aligned} \tag{21}$$

where $\lceil \cdot \rceil$ and $\lfloor \cdot \rfloor$ denote the ceiling and floor functions that round their argument to the next higher or lower integer, respectively. Both (20) and (21) can easily be generated automatically. Figure 5 shows an example root locus plot along with a plot of $C^*(\tilde{s})$ and $K_C(\sigma)$.

5. PERFORMANCE EVALUATION ON A HYDRAULIC TEST SETUP

The proposed controller synthesis approach is applied to a hydraulic test setup that features a KSB Etanorm centrifugal pump (G32-125.1) driven by a 0.55 kW induction motor with frequency converter, which measures the effective motor current $i_{\text{meas}}(t)$. The rotational speed $n(t)$ can be varied between $n_{\min} = 600$ min^{-1} and $n_{\max} = 1500$ min^{-1}. The pump is connected to a piping system with a total length of $L = 11$ m and an average radius of $R = 0.0125$ m. A control valve is placed downstream of the pump to simulate various pipe friction factors and disturbances. The nominal pump operation with a rotational speed $n_{\text{nom}} = 1500$ min^{-1} leads to a nominal flow rate $q_{\text{nom}} = 4.69$ m^3/h (against fully opened control valve). The control algorithms run on a PC with MATLAB that is connected to the process I/Os via PROFIBUS.

We claim the gain K_P can be assumed to be constant in the test setup. This can be seen as follows. The pressures p_0 and p_2 are both approximately equal to atmospheric pressure in the laboratory setup and the geodetic height difference $z_2 - z_1 = 0.5$ m is small, which in particular implies $p_0 \approx p_2^\star$. Since the gain K_P describes the static relationship $K_P = \lim_{t\to\infty} q(t)/n(t)$ after a step in $n(t)$, we may set $dq/dt = 0$ in (3). Using $p_1 = p_D$, which holds according to the assumptions stated in section 3.1, and substituting (6) for p_1 into (3) yields

$$K_P = \lim_{t\to\infty} \frac{q(t)}{n(t)} = \sqrt{\frac{4 \cdot R \cdot A^2 \cdot C_0}{\rho \cdot L \cdot \lambda_f - 4 \cdot R \cdot A^2 \cdot C_2 \cdot n_{\text{nom}}^2}}.$$

The r.h.s. is independent of the point of operation. Figure 3 corroborates that a constant gain K_P does indeed hold for a large range of operating points.

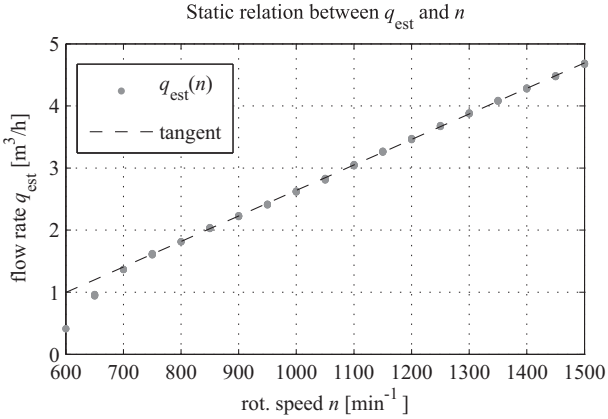

Fig. 3. Static relation between q_{est} and n for a geodetic height difference $z_2 - z_1 = 0.5$ m.

5.1 System identification

Applying the flow rate estimation algorithm results in $T_D = 0.75$ and $T_L = 1.8$ for the process model (12). A rotational speed step from $n_{\text{start}} = 1000$min^{-1} to $n_{\text{end}} = 1100$min^{-1} is performed to determine K_P and T_Q. The resulting time series of $q_{\text{est}}(t)$ is plotted in the left diagram in Fig. 4, where the speed step is performed at $t = 200$ s. K_P can be calculated from the time series of $q_{\text{est}}(t)$ using (10). T_Q results from minimizing (11) with known parameters K_P, T_L and T_D. The right diagram in Fig. 4 shows the mean squared error, i.e., the cost function of (11), with its minimum at $T_Q = 0.55$. In summary, the process model (12) becomes

$$G_P(s) = \frac{0.00449 \cdot e^{-0.75s}}{(1.8s+1)(0.55s+1)}.$$

5.2 Controller synthesis

We choose a standard PI-controller

$$G_C(s) = \frac{K_C \cdot (T_C \cdot s + 1)}{T_C \cdot s}$$

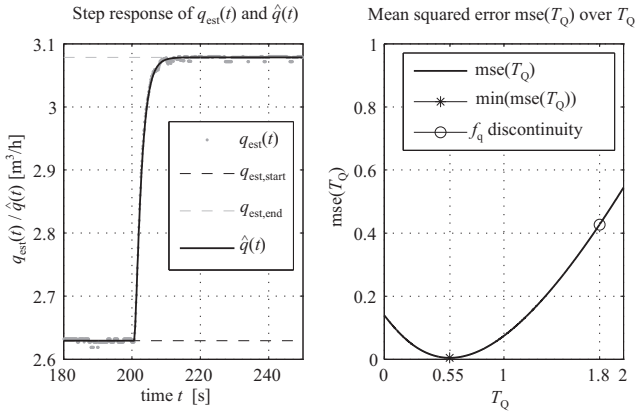

Fig. 4. Left diagram: Estimated flow rate $q_{\text{est}}(t)$ and modeled $\hat{q}(t)$; Right diagram: Cost function of (11). The discontinuity discussed below (11) is marked in the right diagram.

for performance evaluation. The controller time constant T_C is used to compensate the slowest time constant of the process, thus $T_C = T_L$. The open loop transfer function then becomes:

$$G_o(s) = \frac{K_C \cdot 0.00449 \cdot e^{-0.75s}}{0.99s^2 + 1.8s} \tag{22}$$

For the aperiodic limit control the maximum of

$$K_C(s_R) = -\frac{0.99 \cdot s_r^2 + 1.8 s_r}{0.00449 e^{-0.75 \cdot s_R}} \tag{23}$$

has to be determined. This maximum is located between the poles $s_1 = 0$ and $s_2 = -1.\overline{81}$, where $K_C(s_R)$ crosses zero. The lower left diagram in Fig. 5 shows the plot of (23), with a unique maximum at $s_R^* = -0.629$ and controller gain $K_C(s_R^*) = 102.9$. The root locus plot in the upper diagram in Fig. 5 shows the branch point of the two dominant roots located at s_R^* for gain $K_C = 102.9$. Both branches are bend towards the imaginary axis due to the deadtime.

For the ± 45 deg control the first zero crossing of $C^*(\tilde{s})$ (19) has to be detected. Using (20) and (21), $C^*(\tilde{s})$ becomes:

$$C^*(\sigma) = (1.98\sigma^2 - 1.8\sigma) \cdot \cos(T_D \cdot \sigma) + 1.8\sigma \cdot \sin(T_D \cdot \sigma)$$

The lower right diagram in Fig. 5 shows a plot of $C^*(\sigma)$ with a zero crossing at $\sigma^* = 0.529$. The corresponding $K_C(\sigma^*)$ is calculated using the imaginary part of (18), thus

$$K_C(\sigma^*) = \frac{(1.98(\sigma^*)^2 - 1.8\sigma^*)}{K_P \cdot e^{T_D \cdot \sigma^*} \cdot \sin(T_D \cdot \sigma^*)} = 154.1, \tag{24}$$

which is plotted along with $C^*(\sigma)$ in Fig. 5. Note that Fig. 5 shows $K_C(\sigma) \cdot K_P$ instead of $K_C(\sigma)$ for ease of interpretation, which leads to $K_C(\sigma^*) \cdot K_P = 0.692$. The root locus plot in the upper diagram shows the dominant pair of roots located at ± 45 deg for $K_C = 154.1$, thus $s_{1/s} = -0.529 \pm 0.529j$.

5.3 Performance evaluation

We compare four PI controller parameter settings. Settings 1 and 2 result from the root locus based, aperiodic and ± 45 deg, respectively, root location tuning proposed in this paper. Settings 3 and 4 are based on the rules due to Chien, Hrones and Reswick (CHR) for aperiodic setpoint tracking and Ziegler and Nichols's (ZN), respectively. The time

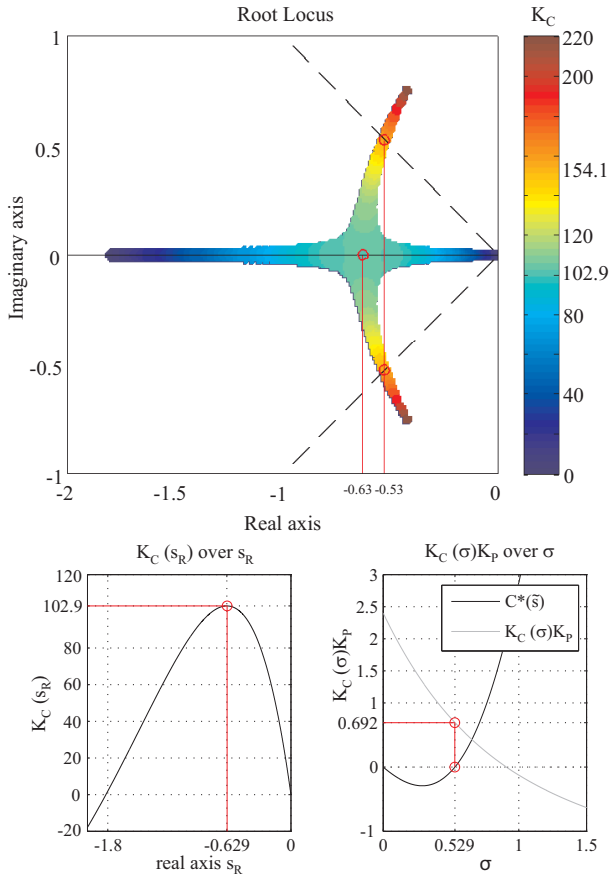

Fig. 5. Root locus plot, $K_C(s_R)$ and $K_C(\sigma) \cdot K_P$ function of the sample process (22)

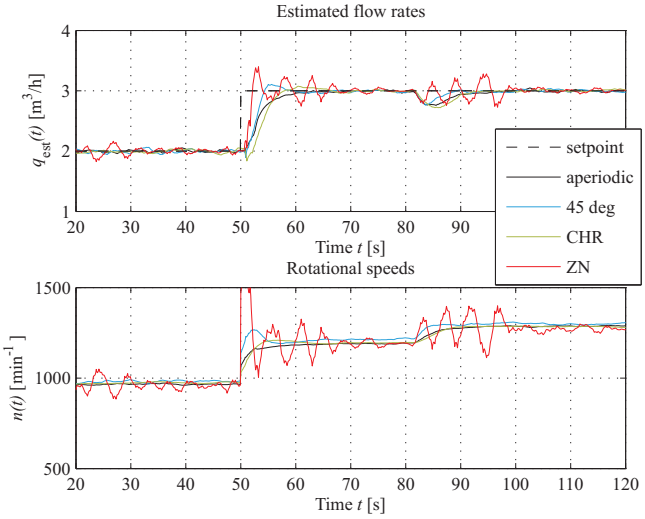

Fig. 6. Performance evaluation of four different PI controller tuning variants.

series in Fig. 6 start with a setpoint at $q_{\text{est}}(t) = 2\text{m}^3/\text{h}$. At $t = 50$s the setpoint is increased to $q_{\text{est}}(t) = 3\text{m}^3/\text{h}$. At $t = 80$s the control valve in the process is partially closed to simulate a disturbance. The results show that the root locus based tuning (settings 1 and 2) provide the desired smooth and robust control, with lower rise time for setting 2. The CHR tuning yields an even lower rise time with a

small overshoot visible on the rotational speed. The ZN tuning leads to aggressive control action, which amplifies the measurement noise, particularly after the disturbance at $t = 80$s. Obviously, the ZN tuning results in the lowest robustness and a minor increase in the process gain will lead to an unstable closed loop control. We define two error measures to assess the control quality quantitatively:

$$\text{MREE} = \frac{1}{\tau}\sum_{k=1}^{\tau}\frac{|q_{\text{est}}(k) - q_{\text{meas}}(k)|}{q_{\text{nom}}};\ \text{MSCE} = \frac{1}{\tau}\sum_{k=1}^{\tau}\varepsilon(k)^2,$$

where τ is the number of measured samples and ε is the control error. The mean squared control error MSCE and the measured energy consumption of the pump are listed in the following table, where we normalize w.r.t. the respective maximum. As expected from Fig. 6 the ZN

Controller setting	MSCE	Energy consumption
Aperiodic root locus	79.84%	94.63%
±45 deg root locus	67.74%	94.78%
CHR	100%	95.95%
ZN	59.9%	100%

tuning shows the lowest MSCE together with the highest energy consumption due to the continued acceleration and deceleration of the pump. Out of settings 1 to 3 the ±45 deg setting shows the lowest MSCE while all three settings have similar energy consumptions that are reduced by approx. 5% w.r.t. the ZN tuning. In order to evaluate the control quality with respect to the estimation quality we compare $q_{\text{meas}}(t)$ and $q_{\text{est}}(t)$ by using the mean, relative estimation error MREE. The results are shown in Fig. 7 for all four controller tunings.

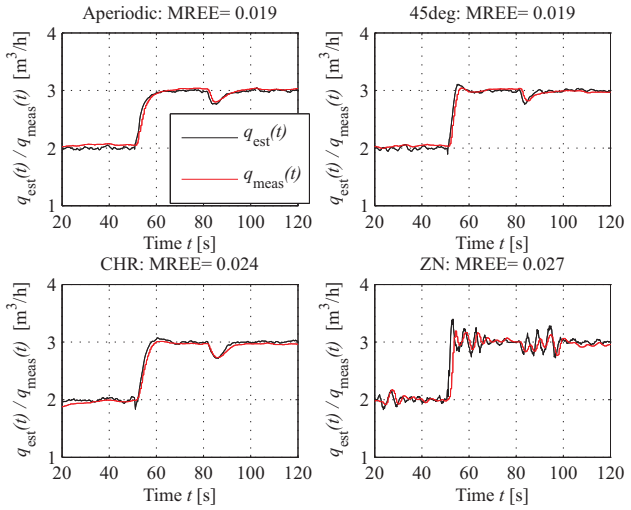

Fig. 7. MREE for all four controller tunings.

The results in Fig. 7 show a reasonable estimation quality that corresponds very well to the measured flow rate, both in steady-state and transient operating conditions.

6. CONCLUSION

We proposed an automatic PID controller tuning approach for flow rate control in low speed radial pumps. The tuning approach and controller do not require an external flow rate sensor. It was the main goal to reduce the implementation effort for the customer to a minimum, which is crucial if the acceptance level of automatic control is to be raised. Although the proposed tuning method requires a process model, the implementation effort is as small as for empirical tuning rules, since the process identification and the controller tuning are fully automated. Unlike empirical tuning rules, our tuning method guarantees a predefined closed loop behavior for delayed systems of arbitrary degree, even for systems with dominant deadtime. The proposed approach proved very useful on a real pumping system.

REFERENCES

T. Ahonen, J. Tamminen, J. Ahola, and J. Kestila. Frequency-converter-based hybrid estimation method for the centrifugal pump operational state. *IEEE Transactions on Industrial Electronics* 59, no. 12 (2012): 4803-4809.

A.T. de Almeida, P. Fonseca, H. Falkner, and P. Bertoldi. Market transformation of energy-efficient motor technologies in the EU. *Energy Policy* 31, no. 6 (2003): 563-575.

C. F. Colebrook. Turbulent flow in pipes, with particular reference to the transition region between the smooth and the rough pipes. *J. Inst. Civ. Eng. London*, volume 11: 133-156.

J. Cvejn. PI/PID Controller Design for FOPDT Plants Based on the Modulus Optimum Criterion. *12th International Carpathian Control Conference (ICCC)* (2011): 60-65.

H. Darcy. Experimental research on the flow of water in pipes (in French). *Comptes rendus des seances de l'Academie des Sciences*, volume 38: 1109-1121.

F. J. T. E. Ferreira, J. A. C. Fong, and A. T. de Almeida. Ecoanalysis of variable speed drives for flow regulation in pumping systems. *IEEE Transactions on Industrial Electronics* 58, no. 6 (2011): 2117-2125.

J. F. Gulich. *Centrifugal pumps*, Springer, 2007.

N. Hohenbichler. All stabilizing PID controllers for time delay systems. *Automatica* 45, no. 11 (2009): 2678-2684.

S. Leonow and M. Mönnigmann. Soft sensor based dynamic flow rate estimation in low speed radial pumps. *Proceedings of the 13th European Control Conference*, Zurich (2013): 778-783.

L. F. Moody. Friction Factors for Pipe Flow. *Transactions of the A.S.M.E.* 66, no. 8 (1944): 671-684.

Q. G. Wang, T. H. Lee, H. W. Fung, Q. Bi and Y. Zhang. PID Tuning for Improved Performance. *IEEE Transactions on Control Systems Technology* 7, no. 4 (1999): 457-465.

J. Weisbach. *Textbook of Engineering Mechanics* (in German), Vieweg, 1848.